Journal of Dynamics, Monitoring and Diagnostics, 2023, 2, 133-143
https://doi.org/10.37965/jdmd.2023.231

ISTP
RESEARCH ARTICLE

Wavelet Denoising Applied to Hardware Redundant Systems for Rolling Element Bearing Fault Detection

Dustin Helm and Markus Timusk
Bharti School of Engineering Laurentian University, Sudbury, Ontario, Canada

(Received 26 March 2023; Revised 05 May 2023; Accepted 05 June 2023; Published online 05 June 2023)

Abstract: This work presents a novel wavelet-based denoising technique for improving the signal-to-noise ratio (SNR) of nonsteady vibration signals in hardware redundant systems. The proposed method utilizes the relationship between redundant hardware components to effectively separate fault-related components from the vibration signature, thus enhancing fault detection accuracy. The study evaluates the proposed technique on two mechanically identical subsystems that are simultaneously controlled under the same speed and load inputs, with and without the proposed denoising step. The results demonstrate an increase in detection accuracy when incorporating the proposed denoising method into a fault detection system designed for hardware redundant machinery. This work is original in its application of a new method for improving performance when using residual analysis for fault detection in hardware redundant machinery configurations. Moreover, the proposed methodology is applicable to nonstationary equipment that experiences changes in both speed and load.

Keywords: fault detection; hardware redundancy; vibration; wavelet denoising

I. INTRODUCTION

A. HARDWARE REDUNDANT SYSTEMS

Hardware redundancy is an important and effective tool in fault-tolerant design of mechanical and electromechanical systems and is often employed to increase reliability and safety in critical systems. The inclusion of multiple redundant components can also increase diagnostic coverage and allow for fault-tolerant design of systems. Hardware redundancy is commonly used for sensor fault detection and accommodation [1,2], in these implementations multiple sensors to measure the same subject. Sensor fault accommodation is the ability of the system to continue operation with a faulty sensor. The International Standards Organisation (ISO) even goes as far as requiring the use of hardware redundancy for safety critical parts of control systems where a certain safety performance level must be met [3]. When implemented for mechanical systems, hardware redundancy often dictates the use of multiple components operating in parallel, where the failure of one will result in increased load on the other remaining healthy components [4], but the overall system is still operational. An example of an industrial application of redundancy is commonly seen in pumping systems where multiple pumps are arranged in parallel, sharing a common load. Such systems are typically designed to continue to operate if one component goes offline. There are many factors to consider when looking at the reliability of redundant systems. Mortazavi *et al.* [5] highlighted the need to consider dependent failures when looking at redundant pump systems. In critical systems (where reliability is important), it is helpful even in highly redundant fault-tolerant systems to obtain usable information on the health of individual components or subsystems.

When considering the application of redundancy in fault detection, one methodology that must be explored is analytical redundancy. These methods employ a mathematical model that is used as a redundant way to determine the value of a measured signal [6]. The relationship between the model and the measured values can take the form of so-called analytical redundancy relations (ARRs). These ARRs are then used to generate residuals that can indicate the state of the machine. The mathematical models used can come in the form of process models or signal models [4]. The form of the generated residuals can be structured such that the fault type can be determined by analyzing the vector composed of the residuals [7]. ARRs were originally developed for linear systems; however, they can be extended to nonlinear systems [8]. More recently, Willersrud *et al.* [9] showed that ARRs can be used to detect incidents while drilling.

Helm and Timusk, [10] have shown that in cases where machinery operates in parallel (such as hardware redundant mechanical systems), it is possible to improve early fault detection accuracy when subsystems are analyzed together instead of as separate systems. In this work, it was shown that by looking at the residual value in the feature domain between two identical subsystems that are linked together to operate identically, it was possible to reduce the fault detection system's sensitivity to the nonstationary machinery operating conditions.

B. CONDITION MONITORING FOR NONSTATIONARY MACHINES

Detection of the early stages of rolling element bearing (REB) failures is an important step when implementing condition-based maintenance schemes for rotating machinery. Due to the many factors that affect the lifetime of REBs and their relatively frequent need for service or replacement, many signal processing techniques have been developed to monitor their condition. One of the most widely used techniques for determining the condition of REBs is the thorough analysis of mechanical vibration. The vibrations produced by rotating machinery can indicate not only

Corresponding author: Markus Timusk (e-mail mtimusk@laurentian.ca).

the health of the machine but also be used to diagnose the type of fault present. Often the signature of an incipient fault is weak when compared to other sources of vibration from adjacent mechanical components (i.e. gears), and this results in a low signal-to-noise ratio (SNR) and requires careful analysis and processing of the vibration signal to extract the needed information. The problem is further complicated when considering machinery that operates in a nonstationary duty cycle such as variable speed and load. This class of machinery generates characteristic signals that are highly variable in time. Due to the transient nature of the fault signature as well as other sources of excitation, applying traditional signal processing techniques to nonstationary signals is a difficult task. Consequently, there is a large body of research aimed at reducing the influence of changes in speed and load from the fault detection process for these nonstationary signals [11]. Some proposed techniques include optimizing the filtering of the signal to increase SNR, time synchronous averaging, as well as the separation of the random fault signatures from the deterministic components in the signal.

When monitoring the vibration of REBs, envelope analysis is perhaps one of the most commonly employed signal processing techniques for fault detection and diagnostics. In this technique, the frequency of amplitude modulations in a high-frequency band of the signal is analyzed to reveal the bearing fault characteristic frequencies [12]. It is generally desirable when applying envelope analysis to perform some preprocessing steps to remove nonfault-related components from the signal. Common techniques such as time synchronous averaging or linear prediction filtering [13,14] can be used to remove the deterministic components from the signal to increase the relative power of the fault signature. This works due to the bearing fault signature's inherently random nature. Techniques such as these can be difficult to apply to nonstationary signals due to the frequency modulation of various components that is inherently present when dealing with signals from nonstationary machinery. This can become even more complicated when considering interactions between angle-dependent (i.e. gear meshing) and time-dependent (characteristics of the signal transfer path) components of the signal.

Many signal processing techniques have been developed to deal with the challenges of monitoring nonstationary machinery. Recently, much research has been focused on the treatment of cyclo-nonstationary signals [15–17] for fault detection. Additionally, there are some methods that extend typical techniques for the separation of deterministic components. One such method is Linear Parameter-Varying Autoregressive Prediction Filtering (LPV-AR). By combining LPV modeling and AR prediction filtering, LPV-AR models can capture the system's dynamic behavior and improve predictions of future values. The varying parameters in the LPV model are estimated using a set of past observations, and the AR model is used to predict future observations based on these estimated parameters. LPV-AR has been used to detect faults in gearboxes [18–20]. Other common techniques include order tracking of the signal to remove frequency modulations that are linked to the rotating frequency of the machine [21], or the analysis of the vibrations in the time-frequency domain to see how the spectral characteristics change over time [22]. Examples of time-frequency domain techniques include wavelet analysis, the Short-Time Fourier Transform (STFT), and empirical mode decomposition. The wavelet transform is a technique that has found many applications for vibration analysis of time-variant systems due to its ability to provide simultaneous localization of signals in the time and frequency domain. The method projects a signal onto a set of orthogonal basis functions to represent the data in the time-frequency domain. Unlike the STFT, the wavelet transform can provide a multiscale time-frequency representation, wherein higher-frequency components are represented with higher time resolution and lower frequencies are represented with higher-frequency resolution.

There are a few different types of wavelet transforms, most notably the continuous wavelet transform (CWT) and the discrete wavelet transform (DWT). The output of the CWT is highly redundant because there is significant overlap between wavelets in each scale. The output of the CWT is an m-by-n matrix where n is the length of the original signal and m is the number of scales (see Fig. 1). The DWT, in contrast, can provide a sparse representation of the original signal, where the number of coefficients is equal to the length of the original signal. The CWT is useful for detailed time-frequency domain analysis, whereas the DWT is commonly used for compression and noise reduction.

The DWT results in a set of coefficients that represent the signal in different frequency bands, with high-frequency components in the detail coefficients and low-frequency

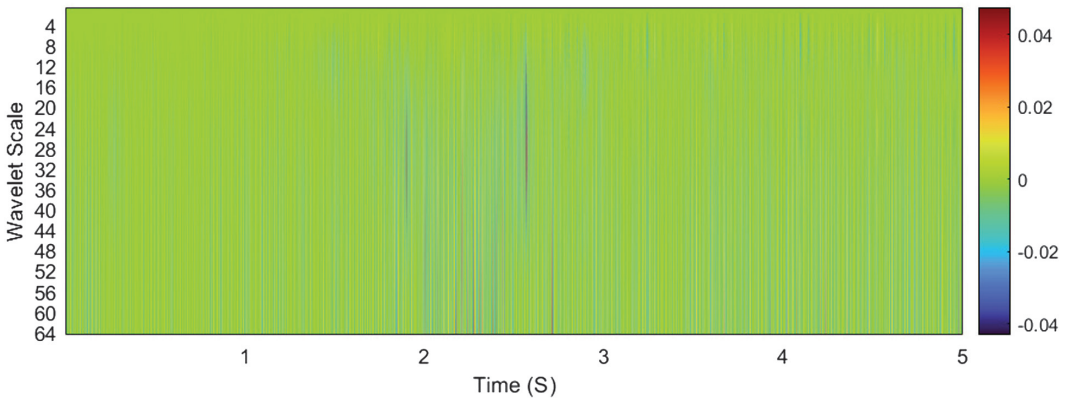

Fig. 1. CWT of a raw vibration signal from a rolling element bearing.

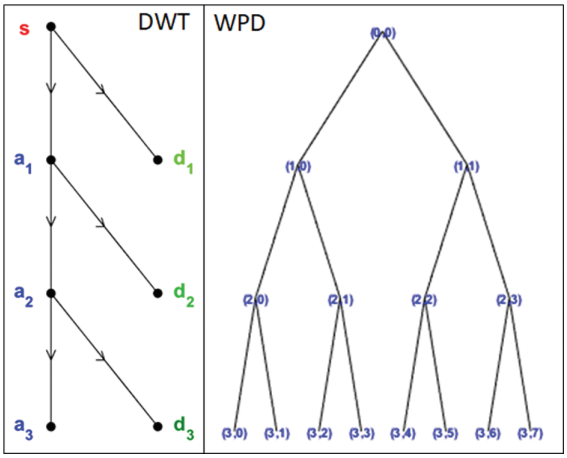

Fig. 2. Three-level decomposition trees for discrete wavelet transform (left) and wavelet packet decomposition (right).

components in the approximation coefficients. The decomposition can be performed recursively, resulting in a multi-resolution analysis of the signal. The DWT only further decomposes the approximation part at each decomposition level.

Another type of transform that has been demonstrated to be effective for condition-based maintenance is wavelet packet decomposition (WPD) [23–25]. WPD is an extension of the DWT that allows for a more flexible decomposition of the signal. In WPD, each node in the decomposition tree has two child nodes, representing the approximation and detail coefficients. The decomposition can be continued recursively, resulting in a tree structure with multiple levels of nodes. The advantage of WPD over DWT is that it provides a more detailed analysis of the signal, allowing for better compression and feature extraction. Figure 2 shows the decomposition tree for both the DWT and WPD.

C. WAVELET DENOISING

First proposed by Mallat [26,27], wavelet denoising is a technique that can be used to help increase the SNR of a raw signal by removing white noise (white noise is defined here as a random series with zero mean and finite variance). In this work, Mallat demonstrated that by using only the local extrema from the wavelet transform modulus, it is possible to reconstruct an approximation of the original signal. This is due to the redundancy of information produced by the wavelet transform. The principal problem in wavelet denoising is the selection of a suitable threshold. Donoho and Johnstone [28] proposed the SureShrink method for wavelet denoising in which the threshold is automatically determined for each decomposition level. Another method was proposed by Cai and Silverman (referred to as the NeighCoeff method) for wavelet denoising. In the NeighCoeff method, neighboring wavelet coefficients are taken into account during the thresholding process [29]. In the more general context, wavelet denoising has been used to denoise bearing vibration signals for the task of fault detection [30–33].

Aminghafari *et al.* [34] extended the typical application of wavelet denoising to multivariate signals. This technique aims to improve denoising results for multivariate signals with additive spatially correlated noise. This method can combine wavelet denoising with principal component analysis (PCA), which is used as a second step to further denoise the signal by leveraging deterministic relationships between the signals. This method addresses systems following the general form of equation 1. Where X is the observed signal that of dimension p, f is the deterministic signal to be recovered, and E is spatially correlated noise:

$$X_p(t) = f_p(t) + E_p(t) \tag{1}$$

This technique has seen some limited applications to fault detection in rotating machinery. Cancan *et al.* proposed a multi-sensor signal denoising scheme based on a matching synchrosqueezing wavelet transform [35]. The technique was implemented to detect faults in gears and bearings using a signal from a three-axis accelerometer. Chaabi *et al.* [36] used this technique to denoise individual intrinsic mode functions (IMFs) generated by Complete Ensemble Empirical Mode Decomposition with Adaptive Noise (CEEMDAN). The denoised IMFs were then analysed using envelope analysis to detect faults in REBs.

Helm and Timusk first proposed an adaption to wavelet denoising aimed specifically at fault detection in hardware redundant systems. This new methodology looked to leverage the information gained when systems are operating in parallel to improve the extraction of weak bearing fault signatures [37]. This technique adapted wavelet denoising to utilize a reference signal for thresholding in the wavelet domain. The results in the original paper were promising; however, the analysis is limited to simulated signals. This work focuses on applying it to real data collected from two mechanically identical subsystems operating in nonstationary conditions, as well as detecting several different fault types. The expectation is that by applying the wavelet denoising algorithm to each of the redundant systems (using the other as a reference), differences in the signals will be amplified and shared deterministic components will be removed. This will result in an increased residual between the two systems in the feature domain making incipient faults easier to detect.

II. METHODOLOGY

A. WAVELET DENOISING USING A REFERENCE SIGNAL

This section describes the proposed methodology used to enhance the relevant information in the measured vibration signals to aid in fault detection and improve the SNR. Unlike typical wavelet denoising applications where measured signals take the form of equation 1 (presented earlier), when implementing denoising for fault detection, we must consider that the signal to be recovered is somewhat random and impulsive in nature. Whereas the "noise" or the parts of the signal that are not related to the fault and need to be eliminated can be deterministic and dominate the signal (such as gear meshing frequencies). When considering hardware redundant systems, similar to the system formulated for multivariate wavelet denoising, there is a deterministic relationship between the measured signals. However, in this case, the relationship is well defined, and the frequency content of the signals (not associated with fault condition) will be the same. While typical

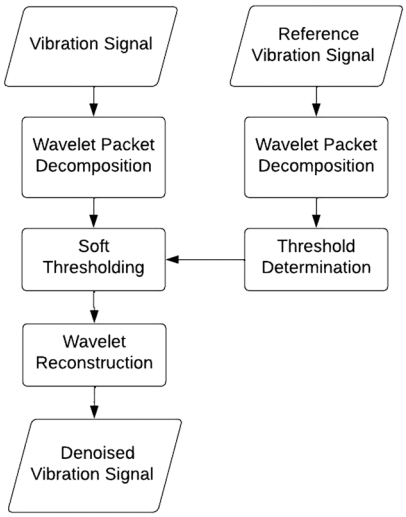

Fig. 3. Wavelet denoising using a reference signal.

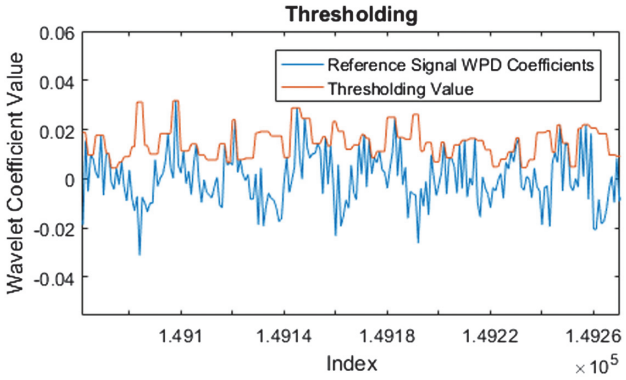

Fig. 4. Wavelet domain threshold determination.

wavelet denoising techniques use a static threshold to remove noise from signals, the proposed technique adapts the thresholding level (in both the scale and time direction) based on information from a reference signal. In doing this, the components of the signals that present the same in the wavelet transform domain can be removed, reducing the original signals to the residuals that are not shared between the two. The steps for the proposed wavelet denoisng methodology are presented in Fig. 3.

The thresholding value for a given scale and index in the wavelet packet transform (WPT) modulus is determined by finding the nearest local maxima of the reference signals WPT modulus at the same scale and index (see Fig. 4).

Soft thresholding is then applied to each signal to remove the shared signal components. See equation 2 for soft thresholding, where x is input, t is the threshold, and y is the output:

$$y = \begin{cases} 0 & \text{if } |x| < t \\ x - t & \text{if } x > t \\ x + t & \text{if } x < -t \end{cases} \tag{2}$$

The signals are then reconstructed using the inverse of the original transform. The reconstructed signals can then be treated with any other suitable fault detection scheme. Additional information on this method can be found in [37].

B. FAULT DETECTION OF HARDWARE REDUNDANT SYSTEMS USING WAVELET DENOISING

When detecting faults in hardware redundant systems, wavelet denoising using a reference signal can be easily employed as the redundant mechanical system can provide the required reference signals. In this application, each of the subsystems can serve as a reference of the other, allowing faults to be detected in either subsystem. When applying this technique to fault detection, the denoised signal must then be analyzed using other methods to determine if there is a fault present. In this work, the denoised signals are analyzed using envelope analysis to extract the bearing fault frequencies and autoregressive (AR) modeling. Features are then extracted from the AR model and the envelope signal, and the resulting feature vectors are compared between the two subsystems to detect the faults. The signal flow of this technique is illustrated in Fig. 5 for depicting both parallel subsystems.

1) WAVELET DENOISING AS APPLIED TO REDUNDANT REBs. After the collection of vibration signals from each subsystem, wavelet denoising is performed using the signal from each subsystem as a reference for the other. In this work, the Fejér–Korovkin wavelet of order 8 was used and the decomposition level was 3. These parameters were initially selected based on the results presented for simulated signals in [38] and then adjusted based on some initial analysis of the resultant denoised signals. In this case, these parameters are not considered to be optimized and should

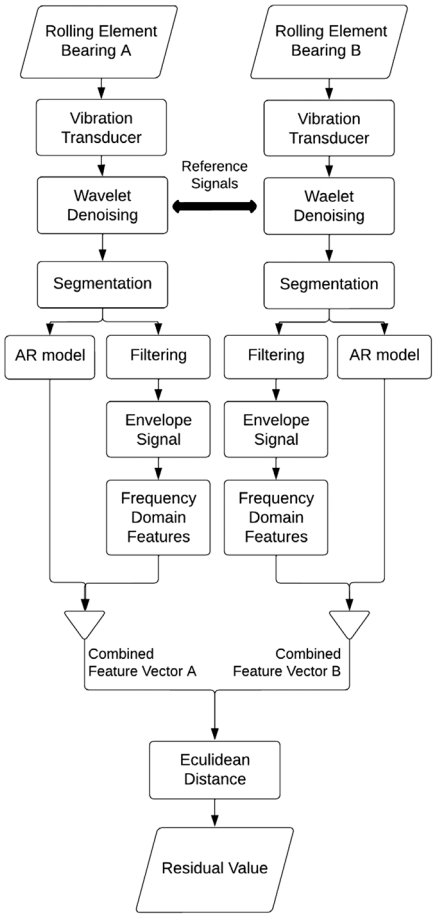

Fig. 5. Flow chart of proposed method.

be chosen for a given system based on a priori knowledge of the system to be analyzed.

2) SEGMENTATION. In an actual industrial application, the vibration signal could reach extreme lengths running continuously for hours. Therefore, it is necessary for fault detection to break them up into shorter manageable chunks for feature extraction. This is achieved using segmentation. Longer segments will be more immune to noise, whereas shorter segments will better localize changes in the nonstationary signals. In this work, the signals were segmented based on an even number of shaft revolutions to ensure each segment contains an appropriate amount of information. This is important in cases where rotating speed varies significantly. For example, at slow speeds the segment must be significantly longer than at high speeds to capture the same number of ball pass events over a potential race fault. In this work, the signals are segmented in parts that contain 10 revolutions of the bearing.

3) FEATURE EXTRACTION FROM DENOISED SIGNALS. For each segment of the signal, a set of features were calculated to represent that given time period. The set of features can be referred to as the feature vector. Two types of features are used in this work: features from envelope analysis and features extracted from AR models. For each segment, an AR model was generated using the Yule–Walker method. The model takes the form of equation 3:

$$y(n) = b_0 x(n) + a_1 y(n-1) + a_2 y(n-2) \ldots a_p y(n-p) \quad (3)$$

The coefficients of the model (a_1–a_p) were used as features to describe the signal. This technique is well known for feature extraction and was chosen due to the model's ability to represent the frequency content of the signal [39–41]. The fit of the model was evaluated using the Akaike information criterion (AIC); see [42]. When optimizing the order of the model (p), there are two competing objectives. The fit of the model to the data used to generate it will improve as the model order increases; however, it is also desirable to keep the dimensionality of the feature space small. A higher-dimensional feature space increases computational requirements, and the available data may become sparse. The AIC with respect to model order for AR models generated for denoised vibration signals is shown in Fig. 6. In this work, the AR models used were order 10. In this case, model order 10 is at the knee of the AIC curve. The AIC presented is the average across tests for several different healthy bearings.

The steps to perform envelope analysis are outlined as part of Fig. 5. First, a bandpass filter is used to filter out the frequency band of interest. The frequency range for filtering was determined by analyzing the kurtogram of the signals. The kurtogram presents the kurtosis (measure of the impulsiveness of the signal) for different frequency bands of the signal (see Fig. 7) [43]. In a signal where a fault is present, the band with the highest kurtosis value can reasonably be assumed to contain the fault signature and therefore be selected for analysis. The frequency band used in this work was from 2000 Hz to 4000 Hz and was obtained using a simple finite impulse response (FIR) bandpass filter. If the structural resonance of the system was known, that could also be used to determine the center frequency for the filter. This is because the ringing caused by the fault is influenced by the structures present along the path of signal transfer.

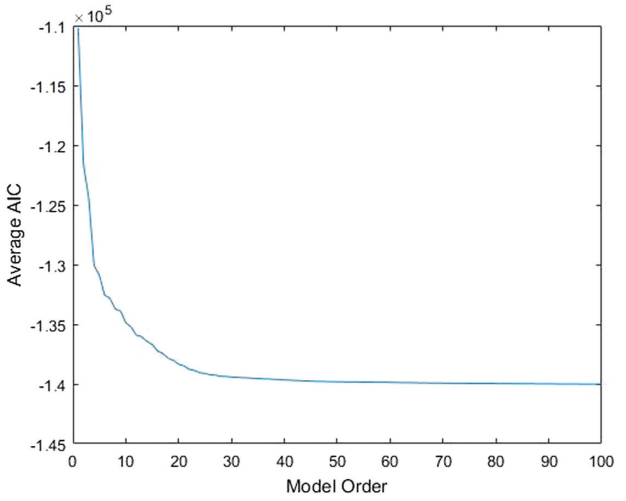

Fig. 6. Mean AIC for AR models generated using a denoised vibration signal.

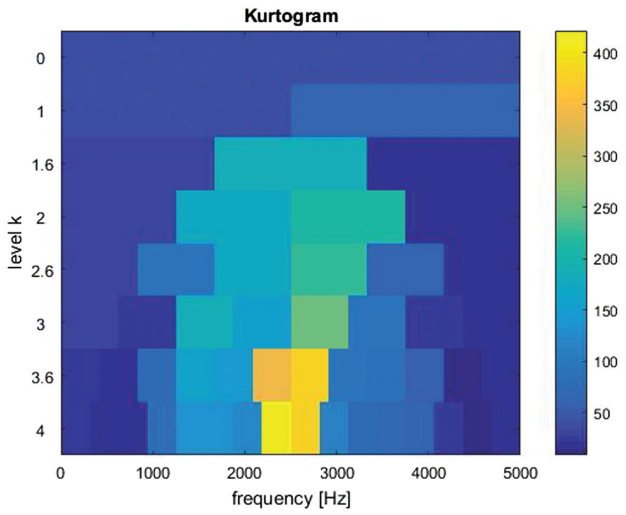

Fig. 7. Kurtogram of a signal after wavelet denoising.

After filtering, the Hilbert transform was used to produce the analytic signal (the complex version of the original real-valued signal without negative frequency components). This is important since without the negative frequency content, the magnitude of the complex analytic signal represents the amplitude of the signal (signal envelope). After the envelope was obtained, a simple Fast Fourier Transform (FFT) could be used to determine the frequency content of the envelope (amplitude modulation frequencies). The features extracted from the envelope frequency spectrum were the difference in magnitude between values found at the ball pass frequency for the inner and outer race, the bearing's rotating frequency, and the rolling element frequency. Additionally, the overall spectral difference was calculated. This measure represents the average spectral dissimilarity or contrast between the envelope amplitudes of two subsystems providing a single quantitative measure of their differences. See equation 4, where *a1(i)* is the amplitude of the envelope of the first subsystem at frequency *i*, *a2(i)* is the same for the second subsystem, and *l* is the length of the spectrum:

$$\text{Spectral Difference} = \frac{\sum_{i=1}^{l} \sqrt{(a_1(i) + a_2(i)) * |a_1(i) - a_2(i)|}}{l} \quad (4)$$

The features were all normalized using the mean and standard deviation of the healthy data. The AR features and envelope features were combined to create a single combined feature vector to represent each time segment. Combining AR features and envelope analysis leverages their respective advantages. The AR features capture the overall signal behavior, while envelope analysis focuses on the fault-specific high-frequency components. Together, they improve the accuracy and reliability of bearing fault detection by capturing both the subtle changes in signal dynamics and the fault-related characteristics.

4) DETECTION OF FAULTS. In order to determine an indicator of the difference between the two bearings, the residual that was calculated between feature vectors from each subsystem was analyzed. The residual represents the overall difference between the two systems in the feature domain. A single residual value or score was calculated based on Euclidean distance of the feature vectors. This represented the magnitude of the distance between the feature vectors in Cartesian space. This distance measure between feature vectors responded to changes in either subsystem that were not common between the two signals (i.e. two vectors that are not the same class will produce a higher Euclidean distance). See equation 5 for the Euclidean distance between N-dimensional feature vectors A and B:

$$\text{Euclidean distance} = \sqrt{(A_1 - B_1)^2 + \ldots (A_N - B_N)^2} \quad (5)$$

This distance was then used to demonstrate the likelihood that there is a fault present. For classification purposes, a threshold on the final residual value was used. Selecting a threshold for detection depends on several factors, including the desired trade-off between false positives and false negatives, and the distribution of the data. In this work, the threshold was set to achieve approximately 10 percent error (false positives) based on a subset of the healthy data. The chosen value is intended to preserve sensitivity to early faults while accounting for the inherent variability among members of the same class, which is influenced by the random characteristics of the systems.

C. DATA COLLECTION

To properly test the proposed methodology, it was required to gather data from bearings in a hardware redundant arrangement. This was achieved using a test bench specifically designed to replicate hardware redundant machinery. Furthermore, it was also required for the machine to operate with a nonstationary duty cycle with independent control of both the speed and load of the components. To achieve these goals, the test setup consisted of two identical belt-driven hydraulic systems that are both driven in parallel with the same control signal. Each of the two subsystems contained a 10-hp induction motor to be used as a drive as well as a hydraulic gear pump to provide the load to the system. The two gear pumps were connected to the same manifold such that they experienced the same hydraulic load. Pressure in the shared manifold was controlled using a solenoid-actuated proportional valve. The variable hydraulic load allowed for controllable variable radial loading of the test bearings as the radial load was caused by the belt tension required to spin the pump pulley. The torque required to spin the pump is directly related to the pressure at the pump output. Gearboxes with a 3:1 reduction and serpentine belts were used to transfer the power from the motors to their respective pumps (see Fig. 8). The motors were controlled using a common variable frequency drive (VFD) and set up to drive each motor at the same speed. The machine was instrumented with pressure sensors, accelerometers, and encoders. The data from the various sensors were collected to be used for fault detection as well as control of the machine. The variable speed and load duty cycle can be seen in Fig. 9.

1) FAULTED COMPONENTS AND DATA COLLECTION. The target mechanical component which was subjected to variable duty in the larger parallel system was a REB in an idler pulley (see Fig. 10). This pulley is located between the load pulley (hydraulic pump) and the drive pulley (connected to the gearbox and motor) on the tension side of the belt drive system. This allowed for modulation of the bearing's speed and load simply by changing the input speed to the system and the pump load. The radial load on the bearing is directly linked to the belt tension and can be determined using the wrap angle and the tension of the belt. The tension in the belt was proportional to the tension due to load torque from the pump, which was variable with respect to pump torque (controlled via hydraulic pressure) plus the

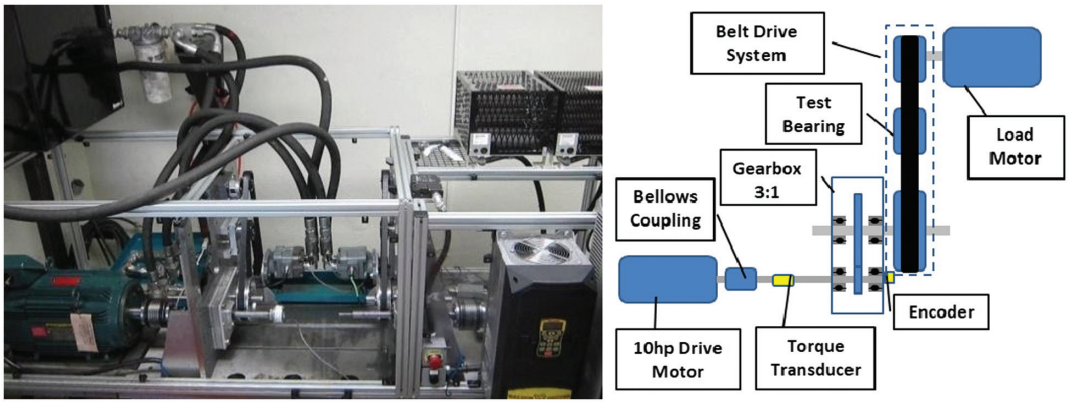

Fig. 8. Parallel machinery simulator.

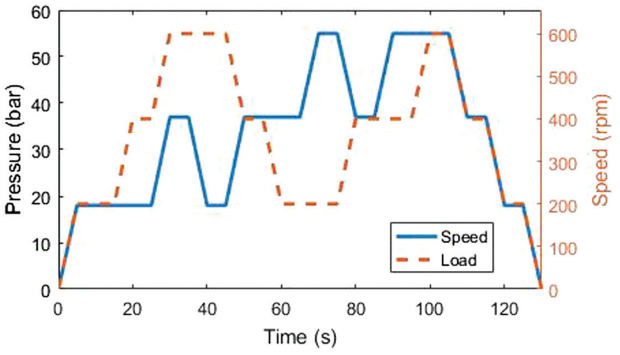

Fig. 9. Machine duty cycle.

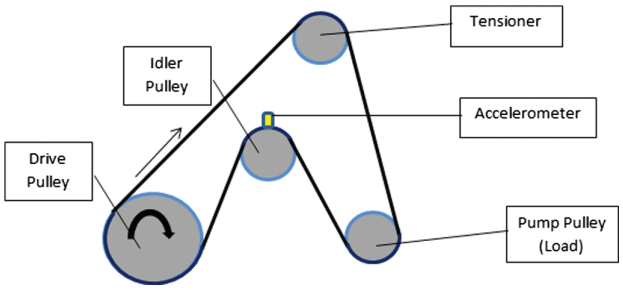

Fig. 10. Belt drive system layout.

initial tension provided by the belt tensioner. The rotational speed of the bearing is proportional to the motor speed factoring in the gearbox ratio and the ratio between the drive pulley and idler pulley diameters. The resulting ratio in this case between the motor and the idler pulley is 1.42:1.

The REBs used in the idler pulleys were deep-groove ball bearings (SKF model 6203) which are commonly used for automotive and automation applications. Mechanical faults were introduced to the contact surfaces inside the bearings using electrical discharge machining (EDM); see Fig. 11. There were three types of faults created: outer race, inner race, and rolling element. The calculated characteristic frequencies associated with these faults can be seen in Table I.

The faults ranged in width from 1.5 mm to 0.25 mm wide. The inner and outer race faults were 0.1 mm deep and covered 2 mm across the bearing surface with a width corresponding to the listed size. The rolling element faults were also 0.1 mm deep. However, they were square with a size corresponding to the listed fault size. In total, 30 tests were run with faulted bearings, once with each fault type in each of the machine's two subsystems. Eight different healthy bearings were also used to collect data with both subsystems in a healthy state as well as for tests in which one of the subsystems contained a fault. Eight tests were run with no fault present. Each test run consisted of one run through a duty cycle of transient speed and load depicted in Fig. 9. Uniaxial accelerometers were mounted to the posts that support the idler pulleys (see Fig. 11 bottom) in a direction aligned with the hub load applied to the pulley. This raw data was collected using a sampling rate of 10 KHz.

Fig. 11. Bearing with outer race fault (top) and assembled in the belt drive system (bottom).

Table I. Bearing characteristic frequencies

Characteristic frequency	Fault order (per bearing revolution)
Ball pass frequency inner (BPFI)	4.947
Ball pass frequency outer (BPFO)	3.053
Fundamental train frequency (FTF)	0.618
Ball spin frequency (BSF)	1.994
Rolling element defect frequency (REDF)	3.988

III. RESULTS

A. WAVELET DENOISING EFFECTS ON ENVELOPE SPECTRUM

In this section, the squared envelope spectrum of a signal encompassing an entire test is shown for both before and after denoising. The reference signal used for the denoising process is a simultaneously collected signal from the other parallel operating subsystem. The top row of Fig. 12 shows these results for a healthy test, and there are many peaks in the envelope of both the original and the denoised signal. However, note that the magnitude of peaks in the denoised signal decreases by a factor of about 10.

Figure 13 shows the same results for a signal from a bearing with a 1.5-mm inner race fault. In this case, the spectrum from the original signal appears very similar to that of the healthy test. However, the denoised spectrum contains one clear peak that is located at the ball pass order

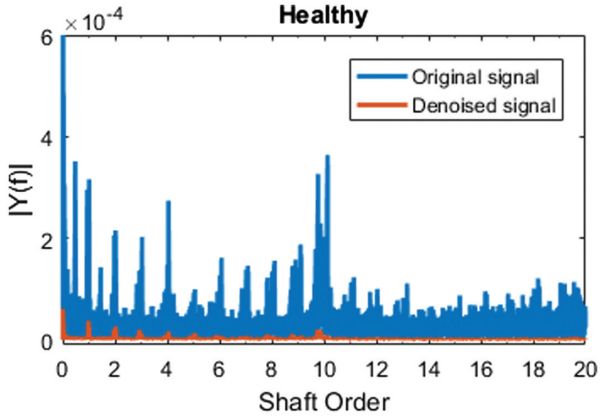

Fig. 12. Envelope spectrum of the original and the denoised signals for a healthy bearing.

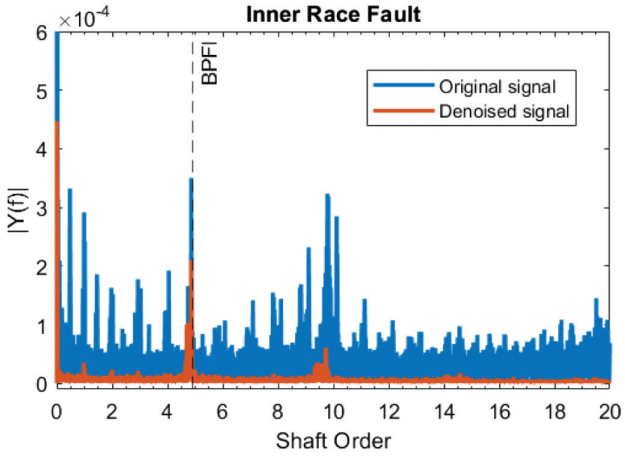

Fig. 13. Envelope spectrum of the original and the denoised signals for a 1.5-mm inner race fault.

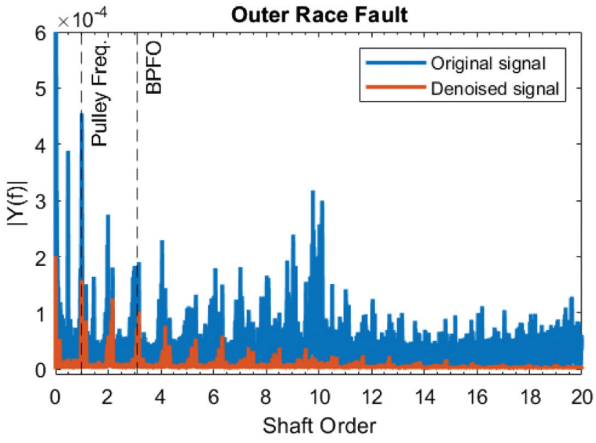

Fig. 14. Envelope spectrum of the original and the denoised signals for a 1.5-mm outer race fault.

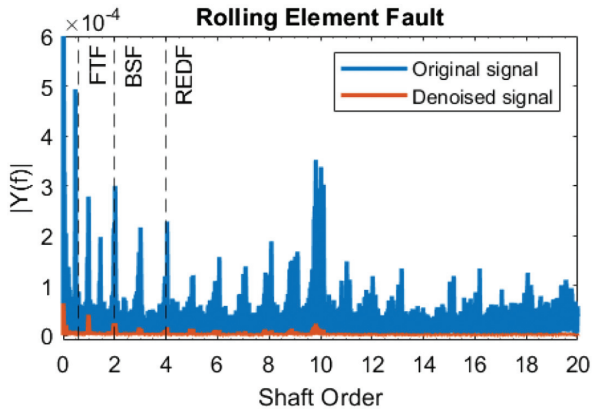

Fig. 15. Envelope spectrum of the original and the denoised signals for a 1.5-mm rolling element fault.

for the inner race. Since in the case of an idler pulley, the inner race of the bearing is stationary, no modulations at the pulley's rotational frequency are expected (unlike many applications, gearboxes for example). Moreover, the peak at the ball pass frequency is expected to be pronounced, since the fault is in the load zone of the bearing at all times.

A similar type of result for a bearing with a 1.5-mm outer race fault can be seen in Fig. 14. In this case, the spectrum of the original signal again looks the same as the healthy case. However, the denoised spectrum has peaks that correspond to the pulleys rotational frequency and its harmonics. This is to be expected because in this case, the fault is moving in and out of the load zone due to the rotation of the pulley housing.

Finally, Fig. 15 illustrates the results for a 1.5-mm rolling element fault. These results look similar to the healthy case for both the original and the denoised signal. This is not a promising result; however, it is expected that the rolling element fault is the most difficult to detect in any case since each rolling element will spend significant time outside the load zone of the bearing and there are orientations of the rolling element in which the fault (if small enough) will not contact the bearing race. Furthermore, this is in line with other results found using the same data set [44].

B. CLASSIFICATION RESULTS USING RESIDUAL ANALYSIS

For classification, a simple thresholding method was used on the Euclidean distance values obtained for each segment of the data. As described earlier, this distance value will trend up when a fault is present in either subsystem. Therefore, to assess the likelihood that a fault is present, we must look at the number of segments that have a distance above a set threshold. In this work, the threshold was set based on analysis of the healthy data only. It was set such that it would include all but the highest 10 percent of the healthy data. In this work, results are presented for the proposed methodologies both with and without the wavelet denoising step. In this manner, it is possible to determine the value added to the fault detection architecture by using the proposed parallel wavelet denoising methodology. Results over an entire range of threshold values can be seen in Fig. 16. This shows the receiver operating characteristic (ROC) curve for the 1.5-mm inner race fault both with and without denoising. The ROC curve plots the outliers rejected (fraction of faulted segments that exceed the threshold value) versus the targets accepted (fraction of healthy segments that fall under the threshold) as the threshold value changes. Figure 16 plots this result for the same data

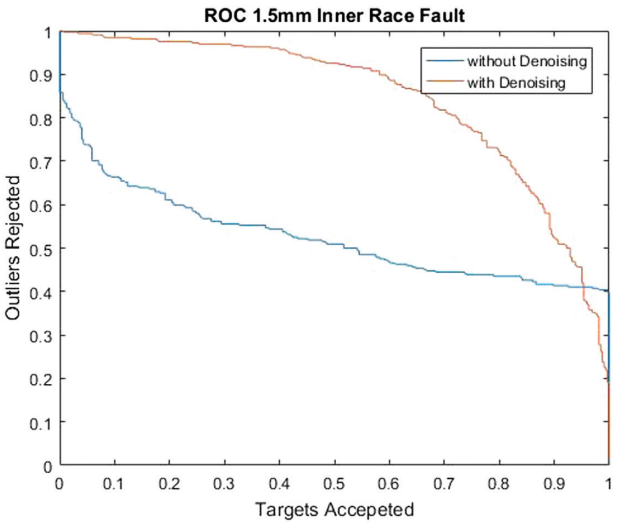

Fig. 16. ROC plot for 1.5-mm inner race fault.

Table II. Classification error rate for healthy tests (% false positives)

Case	With denoising	Without denoising
Test #1	29	18.7
Test #2	9.3	7.2
Test #3	4.1	4.1
Test #4	3.13	18.8
Test #5	3.1	4.1
Test #6	10.2	0
Test #7	10.1	14.3
Test #8	10.3	11.3

both with and without the wavelet denoising step, and it can clearly be seen here that the denoising step improves the result.

Tables II and III list the classification results for the healthy and faulted tests, respectively. The results are given in terms of the error rates of false positives and false negatives. The error rate for the healthy tests is considered to be the percent of segments that have a residual that exceeds the threshold value. Likewise for the faulted tests, the error rate is the percent of segments that have a residual that falls under the threshold. On average, both systems performed reasonably well, while the denoising technique provided a noticeable improvement with the inner and outer race faults. The denoising technique did not offer a performance improvement on the rolling element fault. However, the rolling element fault was not well detected in either case. The results did not exhibit a strict trend in relation to fault size. Nevertheless, as expected, the general tendency is for the accuracy of detection to increase as the fault sizes become larger. It is important to acknowledge that the five fault sizes examined were relatively small, representing only incipient bearing faults. Thus, it is anticipated that more severe faults or a wider range of fault sizes would significantly amplify this trend.

Table III. Classification error rates for faulted tests (% false negatives)

Fault size (mm)	With denoising	Without denoising
Outer race fault		
0.25	35.4	43.2
0.5	19.7	24
0.75	14.6	37.5
1	21.9	34.6
1.5	19.6	21.8
Inner race fault		
0.25	14	15.6
0.5	4.7	8.9
0.75	13.4	15.6
1	10.8	16
1.5	11.3	18.6
Rolling element fault		
0.25	87	75
0.5	84	64
0.75	83.8	75.5
1	86.5	77.1
1.5	67.7	67.7

IV. CONCLUSIONS

This work proposes the application of a novel parallel wavelet denoising technique for the detection of faults in hardware redundant mechanical systems. The proposed wavelet denoising method provided a noticeable improvement in ability to detect incipient bearing race faults in a parallel system as compared to the same architecture implemented without this denoising step. However, the wavelet denoising technique did not appear to improve the results for the rolling element faults. It is important to note that the rolling element fault was not well detected in either case. The proposed system was not optimized, and future work should include a methodology or rationale for optimizing the parameters associated with wavelet denoising, namely decomposition level and choice of wavelet. Future work should also look at different nonstationary mechanical systems where frequency characteristics are variable.

CONFLICT OF INTEREST STATEMENT

The authors declare no conflicts of interest.

References

[1] M. M. Gor, P. M. Pathak, A. K. Samantaray, J.-M. Yang, and S. W. Kwak, "Fault accommodation in compliant quadruped robot through a moving appendage mechanism," *Mech. Mach. Theory*, vol. 121, pp. 228–244, 2018.

[2] K. Medjaher, A. K. Samantaray, B. Ould Bouamama, and M. Staroswiecki, "Supervision of an industrial steam generator. Part II: online implementation," *Control Eng. Pract.*, vol. 14, no. 1, pp. 85–96, 2006.

[3] "Safety of machinery — Safety-related parts of control systems — Part 1: general principles for design," *ISO Standard*, vol. 13849–1, 2015. https://www.iso.org/standard/69883.html.

[4] R. Isermann, "Fault-diagnosis systems: an introduction from fault detection to fault tolerance," *Fault-Diagn. Syst.: An Introd. Fault Detect. Fault Tolerance*, (1st ed.), pp. 1–475, 2006.

[5] S. M. Mortazavi, M. Mohamadi, and J. Jouzdani, "MTBF evaluation for 2-out-of-3 redundant repairable systems with common cause and cascade failures considering fuzzy rates for failures and repair: a case study of a centrifugal water pumping system," *J. Ind. Eng. Int.*, vol. 14, no. 2, pp. 281–291, 2018.

[6] R. Isermann and P. Ballé, "Trends in the application of model-based fault detection and diagnosis of technical processes," *Control Eng. Pract.*, vol. 5, no. 5, pp. 709–719, 1997.

[7] J. Gertler, "Fault detection and isolation using parity relations," *Control Eng. Pract.*, vol. 5, no. 5, pp. 653–661, 1997.

[8] M. Staroswiecki and G. Comtet-Varga, "Analytical redundancy relations for fault detection and isolation in algebraic dynamic systems," *Automatica*, vol. 37, no. 5, pp. 687–699, 2001.

[9] A. Willersrud, M. Blanke, and L. Imsland, "Incident detection and isolation in drilling using analytical redundancy relations," *Control Eng. Pract.*, vol. 41, pp. 1–12, 2015.

[10] D. Helm and M. Timusk, "Fault detection for parallel operating machines," *J. Qual. Maint. Eng.*, vol. 26, no. 2, pp. 335–348, 2019.

[11] A. Anwarsha and T. N. Babu, "Recent advancements of signal processing and artificial intelligence in the fault detection of rolling element bearings: a review," *J. Vibroeng.*, vol. 24, no. 6, pp. 1027–1055, 2022.

[12] R. B. Randall, "State of the art in monitoring rotating machinery – part 1," *Sound Vib.*, vol. 38, no. 3, pp. 14–21 +13, 2004.

[13] S. M. Kay and S. L. Marple Jr., "Spectrum analysis – a modern perspective," *Proc. IEEE*, vol. 69, no. 11, pp. 1380–1419, 1981.

[14] P. D. McFadden and M. M. Toozhy, "Application of synchronous averaging to vibration monitoring of rolling element bearings," *Mech. Syst. Signal Process.*, vol. 14, no. 6, pp. 891–906, 2000.

[15] K. Gryllias, S. Moschini, and J. Antoni, "Application of cyclo-non-stationary indicators for bearing monitoring under varying operating conditions," *Proc. ASME Turbo Expo*, vol. 6, 2017. doi: 10.1115/1.4037638.

[16] D. Abboud, S. Baudin, J. Antoni, D. Remond, M. Eltabach, and O. Sauvage, "The spectral analysis of cyclo-non-stationary signals," *Mech. Syst. Signal Process.*, vol. 75, pp. 280–300, 2016.

[17] D. Abboud, J. Antoni, S. Sieg-Zieba, and M. Eltabach, "Envelope analysis of rotating machine vibrations in variable speed conditions: a comprehensive treatment," *Mech. Syst. Signal Process.*, vol. 84, pp. 200–226, 2017.

[18] Y. Chen, X. Liang, and M. J. Zuo, "Sparse time series modeling of the baseline vibration from a gearbox under time-varying speed condition," *Mech. Syst. Signal Process.*, vol. 134, 2019. doi: 10.1016/j.ymssp.2019.106342.

[19] Y. Chen, S. Schmidt, P. S. Heyns, and M. J. Zuo, "A time series model-based method for gear tooth crack detection and severity assessment under random speed variation," *Mech. Syst. Signal Process.*, vol. 156, 2021. doi: 10.1016/j.ymssp.2020.107605.

[20] Y. Chen and M. J. Zuo, "A sparse multivariate time series model-based fault detection method for gearboxes under variable speed condition," *Mech. Syst. Signal Process.*, vol. 167, 2022. doi: 10.1016/j.ymssp.2021.108539.

[21] R. B. Randall and J. Antoni, "Rolling element bearing diagnostics-a tutorial," *Mech. Syst. Signal Process.*, vol. 25, no. 2, pp. 485–520, 2011.

[22] A. Prudhom, J. Antonino-Daviu, H. Razik, and V. Climente-Alarcon, "Time-frequency vibration analysis for the detection of motor damages caused by bearing currents," *Mech. Syst. Signal Process.*, vol. 84, pp. 747–762, 2017.

[23] Q. Hu, A. Qin, Q. Zhang, J. He, and G. Sun, "Fault diagnosis based on weighted extreme learning machine with wavelet packet decomposition and KPCA," *IEEE Sens. J.*, vol. 18, no. 20, pp. 8472–8483, 2018.

[24] L. Huang, H. Huang, and Y. Liu, "A fault diagnosis approach for rolling bearing based on wavelet packet decomposition and GMM-HMM," *Int. J. Acoust. Vib.*, vol. 24, no. 2, pp. 199–209, 2019.

[25] S. Schmidt, P. S. Heyns, and K. C. Gryllias, "A discrepancy analysis methodology for rolling element bearing diagnostics under variable speed conditions," *Mech. Syst. Signal Process.*, vol. 116, pp. 40–61, 2019.

[26] S. Mallat, "Zero-crossings of a wavelet transform," *IEEE Trans. Inf. Theory*, vol. 37, no. 4, pp. 1019–1033, 1991.

[27] S. Mallat and W. L. Hwang, "Singularity detection and processing with wavelets," *IEEE Trans. Inf. Theory*, vol. 38, no. 2 pt II, pp. 617–643, 1992.

[28] D. L. Donoho and I. M. Johnstone, "Adapting to unknown smoothness via wavelet shrinkage," *J. Am. Stat. Assoc.*, vol. 90, no. 432, pp. 1200–1224, 1995.

[29] T. T. Cai and B. W. Silverman, "Incorporating information on neighbouring coefficients into wavelet estimation," *Sankhya Indian J. Stat., Series B (1960–2002)*, vol. 63, no. 2, pp. 127–148, 2001.

[30] H. Qiu, J. Lee, J. Lin, and G. Yu, "Wavelet filter-based weak signature detection method and its application on rolling element bearing prognostics," *J. Sound Vib.*, vol. 289, no. 4–5, pp. 1066–1090, 2006.

[31] E. M. Bertot, P.-P. Beaujean, and D. Vendittis, "Refining envelope analysis methods using wavelet de-noising to identify bearing faults," *Eur. Conf. PHM Soc.*, vol. 2, pp. 119–126, 2014.

[32] L. Zhen, H. Zhengjia, Z. Yanyang, and W. Yanxue, "Customized wavelet denoising using intra- and inter-scale dependency for bearing fault detection," *J. Sound Vib.*, vol. 313, no. 1–2, pp. 342–359, 2008.

[33] C. Mishra, A. K. Samantaray, and G. Chakraborty, "Rolling element bearing defect diagnosis under variable speed operation through angle synchronous averaging of wavelet de-noised estimate," *Mech. Syst. Signal Process.*, vol. 72–73, pp. 206–222, 2016.

[34] M. Aminghafari, N. Cheze, and J.-M. Poggi, "Multivariate denoising using wavelets and principal component analysis BT - Statistical Signal Extracting and Filtering," *Comput. Stat. Data Anal.*, vol. 50, no. 9, pp. 2381–2398, 2006.

[35] C. Yi, Y. Lv, H. Xiao, T. Huang, and G. You, "Multisensor signal denoising based on matching synchrosqueezing wavelet transform for mechanical fault condition assessment," *Meas. Sci. Technol*, vol. 29, no. 4, 2018. doi: 10.1088/1361-6501/aaa50a.

[36] L. Chaabi, A. Lemzadmi, A. Djebala, M. L. Bouhalais, and N. Ouelaa, "Fault diagnosis of rolling bearings in non-stationary running conditions using improved CEEMDAN and multivariate denoising based on wavelet and principal component analyses," *Int. J. Adv. Manuf. Techn.*, vol. 107, no. 9–10, pp. 3859–3873, 2020.

[37] D. Helm and M. Timusk, "Extraction of weak bearing fault signatures from non-stationary signals using parallel wavelet denoising," in *Adv. Condit. Monit. Mach. Non-station. Oper.: Proc. 6th Int. Conf. Condit. Monit. Mach. Non-Station. Oper.*, Springer International Publishing, 2018, pp. 3–11, 2019. doi: 10.1007/978-3-030-11220-2_1.

[38] D. Helm and M. Timusk, "Extraction of weak bearing fault signatures from non-stationary signals using parallel wavelet denoising," vol. 15, 2019. doi: 10.1007/978-3-030-11220-2_1.

[39] J. McBain and M. Timusk, "Feature extraction for novelty detection as applied to fault detection in machinery," *Pattern Recogn. Lett.*, vol. 32, no. 7, pp. 1054–1061, 2011.

[40] M. Timusk, M. Lipsett, and C. K. Mechefske, "Fault detection using transient machine signals," *Mech. Syst. Signal Process.*, vol. 22, no. 7, pp. 1724–1749, 2008.

[41] T. Han and D. Jiang, "Rolling bearing fault diagnostic method based on VMD-AR model and random forest classifier," *Shock Vib.*, vol. 2016, 2016. doi: 10.1155/2016/5132046.

[42] E. Figueiredo, J. Figueiras, G. Park, C. R. Farrar, and K. Worden, "Influence of the autoregressive model order on damage detection," *Comput.-Aid. Civil Infrastruct. Eng.*, vol. 26, no. 3, pp. 225–238, 2011.

[43] J. Antoni, "Fast computation of the kurtogram for the detection of transient faults," *Mech. Syst. Signal Process.*, vol. 21, no. 1, pp. 108–124, 2007.

[44] D. Helm and M. Timusk, "Using residual analysis for the detection of faults in unsteadily operating rolling element bearings," in BINT First World Congr. Condit. Monit. (WCCW), 2017.